Photostriction in Ferroelectrics from Density Functional Theory

Charles Paillard,[1,2,*] Bin Xu,[2,3] Brahim Dkhil,[1] Grégory Geneste,[4] and L. Bellaiche[2,3]
[1]Laboratoire Structures, Propriétés et Modélisation des Solides, CentraleSupélec, CNRS UMR8580, Université Paris-Saclay, 92290 Châtenay-Malabry, France
[2]Physics Department, University of Arkansas, Fayetteville, Arkansas 72701, USA
[3]Institute for Nanoscience and Engineering, University of Arkansas, Fayetteville, Arkansas 72701, USA
[4]CEA, DAM, DIF, F-91297 Arpajon France
(Received 12 February 2016; published 13 June 2016)

An *ab initio* procedure allowing the computation of the deformation of ferroelectric-based materials under light is presented. This numerical scheme consists in structurally relaxing the system under the constraint of a fixed n_e concentration of electrons photoexcited into a specific conduction band edge state from a chosen valence band state, via the use of a constrained density functional theory method. The resulting change in lattice constant along a selected crystallographic direction is then calculated for a reasonable estimate of n_e. This method is applied to bulk multiferroic $BiFeO_3$ and predicts a photostriction effect of the same order of magnitude than the ones recently observed. A strong dependence of photostrictive response on both the reached conduction state and the crystallographic direction (along which this effect is determined) is also revealed. Furthermore, analysis of the results demonstrates that the photostriction mechanism mostly originates from the screening of the spontaneous polarization by the photoexcited electrons in combination with the inverse piezoelectric effect.

DOI: 10.1103/PhysRevLett.116.247401

The coupling of ferroelectric or multiferroic materials with light is currently attracting a lot of attention [1], as, e.g., demonstrated by the above-band-gap photovoltages found in $BiFeO_3$ (BFO) thin films [2], the search of low band gap materials for photovoltaic applications [3], or the recent development in the so-called hybrid perovskite solar cells [4]. Beyond the photovoltaic effect, there is another coupling between light and properties of ferroelectrics or multiferroics that is of current interest, namely, the so-called *photostriction* effect, a deformation of the material under illumination [5]. The photostriction phenomenon opens new perspectives for combining several functionalities in future generations of remote switchable devices and is promising for the realization of light-induced actuators [5]. It has been recently observed in BFO under visible light [6,7]. A giant shear strain generated by femtosecond laser pulses was also reported [8,9], and time-resolved synchrotron diffraction reported a shift of the Bragg peak on a picosecond time scale in both bismuth ferrite [10] and lead titanate [11]. However, the microscopic mechanism responsible for photostriction is poorly understood [8,9]. Obviously, having accurate numerical techniques able to tackle photostriction will allow us to "shed some light" on this effect. However, to the best of our knowledge, such numerical tools allowing a systematic study of the photostriction phenomenon and its atomistic origin are not available yet, despite recent attempts to use Density Functional Theory (DFT) as a tool to fit x-ray absorption spectra in pump-probe photostriction experiments [12].

Here, we report the development of an *ab initio* procedure to compute photostriction from first principles. This procedure not only reproduces the order of magnitude of the observed change of lattice constant in BFO [6], but also reveals that photostriction mostly originates from the combination of the screening of the polarization by the electrons photoejected in the conduction band and the inverse piezoelectric effect. It is also found that photostriction depends on the precise conduction state the electron is excited into, and on the crystallographic direction along which the effect is studied.

In order to realize the difficulty in mimicking photostriction, let us start by recalling that the Kohn-Sham (KS) implementation of DFT [13] reformulates the many-body problem of interacting electrons into many single-body problems, and "only" guarantees that the model noninteracting KS Hamiltonian yields the same *ground state* density and energy as the real interacting Hamiltonian. Such a fact, therefore, leaves the description of unoccupied states within traditional DFT an unanswered question, and the determination of excitation energies remains the privilege of rather costly techniques, such as time-dependent DFT [14] or the *GW* approximation [15]. However, an alternative formulation of DFT that treats ground and excited states on the same footing has been proposed [16]. In particular, Ref. [16] connected each eigenstate of a real interacting Hamiltonian with the eigenstate of a model noninteracting Hamiltonian through a generalized adiabatic connection (GAC) scheme. The so-called ΔSCF method [17] takes advantage of this GAC scheme, and assumes an one-to-one correspondence between the excited states of a single Kohn-Sham system and the real system [16]. This ΔSCF scheme has proved successful and computationally

efficient in, e.g., describing resonance levels of molecules adsorbed on metallic surfaces [18], or the ligand-field splitting of Fe d-orbitals in Fe-phtalocyanine [19] or excited impurity states of chromium in Al_2O_3 [20]. Technically, by introducing constraint fields μ_i, the ΔSCF approach forces the population of the Kohn-Sham eigenstate to be close to a preselected value, via the minimization of the functional [19]:

$$E[n(\boldsymbol{r})] = E_{\mathrm{DFT}}[n(\boldsymbol{r})] + \sum_i \mu_i |n_i - N_i|, \qquad (1)$$

where $n(\boldsymbol{r})$ is the electronic density, $E_{\mathrm{DFT}}[n(\boldsymbol{r})]$ is the usual Kohn-Sham functional, n_i is the occupation number of the ith eigenstate to be constrained, and N_i is the value of the desired constrained occupation number.

In order to describe both the ground and the excited states of $BiFeO_3$ within the ΔSCF method we used the ABINIT code [21] within the PAW framework [22], employing the Local Spin Density Approximation+U (LSDA + U) functional, with $U = 3.87$ eV [23]. Calculations were run on a 10-atom antiferromagnetic rhombohedral cell of BFO, with no spin-orbit coupling interaction being considered. A $10 \times 10 \times 10$ k-point mesh is used here. Structural convergence (ground and excited states) is achieved when the force on any atom is less than 2.5×10^{-6} eV/Å, while self-consistency of the electronic density is considered to be reached when the difference of the force on each atom between two subsequent self-consistent field iterations is smaller than 5×10^{-8} eV/Å.

The predicted relaxed $R3c$ ground state of BFO has a rhombohedral lattice constant of 5.535 Å and a rhombohedral angle of 59.68°, which is consistent with both the values of 5.52 Å and 59.84° found in previous LSDA + U calculations (with U = 4 eV) [24], and the experimental data of 5.63 Å and 59.3° [25]—especially, once recalling the typical 1%–2% underestimation of the lattice constant by LSDA. Regarding the study of excited states within ΔSCF, both the population of the highest occupied KS eigenstates and the lowest unoccupied KS eigenstates are forced manually, which accounts for using an almost infinite constraint field in Eq. (1). Structural relaxation within these fixed constraints are then performed.

Let us first concentrate on the computed band structure of the $R3c$ ground state of BFO, which is shown in Fig. 1. The electronic band gap is equal to 2.05 eV, in agreement with earlier computational work [24], but, as is well known for DFT calculations, is an underestimate of the band gap of 2.67 eV measured in single crystals [26]. This band gap is indirect, with the valence band maximum (VBM) lying in-between the high symmetry B and Z points of the first Brillouin zone, while the conduction band minimum (CBM) occurs at the high symmetry Z point (see, e.g., Fig. 14 of Ref. [27] for a sketch of the first Brillouin zone). As a result and as further indicated in Fig. 1, we consider here three types of excitations: a first one denoted as direct

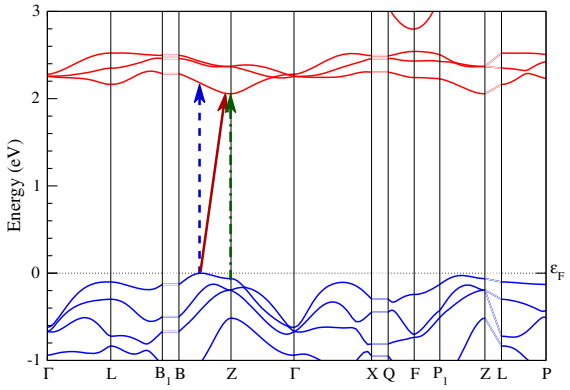

FIG. 1. Computed band structure of $BiFeO_3$ in its $R3c$ ground state. Arrows show the "direct VBM" transition (dashed blue), the "indirect VBM-CBM" transition (red), and the "direct CBM" transition (dotted-dashed green). The zero of energy is chosen at the VBM.

VBM and that leaves holes close to the VBM while bringing electrons at the same k points in the conduction band (see the dashed blue arrow in Fig. 1); the direct CBM, which mimics the vertical transition that adds electrons at or close to the CBM and leaves holes at the same points in the valence band (dotted green arrow); and, finally, the indirect VBM-CBM transition that results in holes at the VBM and electrons at the CBM (red arrow). Note that pump-probe experiments show that the typical electron-phonon interaction, responsible for thermal relaxation of the excited electrons to the CBM, is quickly achieved within 1 ps [28], while recombination rates determined by scanning probe photoinduced transient spectroscopy were estimated to be 75 μs and 1.5 ms in BFO [29]. Similar arguments should hold for relaxation of the holes towards the VBM. Hence, the most likely photon absorption scenario is the indirect VBM-CBM transition. However, for the sake of completeness, we also study in detail the direct VBM and direct CBM optical transitions here.

Figure 2 shows different predicted properties in the $R3c$ state of BFO as a function of the concentration of excited electrons, n_e, for these three transitions. Such concentration is practically allowed here to vary from 0 (ground state) to 5×10^{20} electrons per cm^3—as we excite a maximum of 60 electrons within a $10 \times 10 \times 10$ k-point mesh, which is equivalent to excite 60 electrons in a volume of $10 \times 10 \times 10$ unit cells due to periodic boundary conditions. Figures 2(a) and 2(b) reveal that, for all studied transitions, the pseudocubic lattice constant a_{pc} (i.e., along the pseudocubic ⟨001⟩ directions), linearly shrinks with the excited electron concentration while the pseudocubic angle α_{pc} adopts an opposite behavior, and linearly increases towards the ideal cubic value of 90° (note that such a linear trend of the lattice constant has been observed in time-resolved XRD experiments [30], which attests to the accuracy and relevance of our numerical method). Interestingly, these changes for both the pseudocubic lattice constant and angle are more

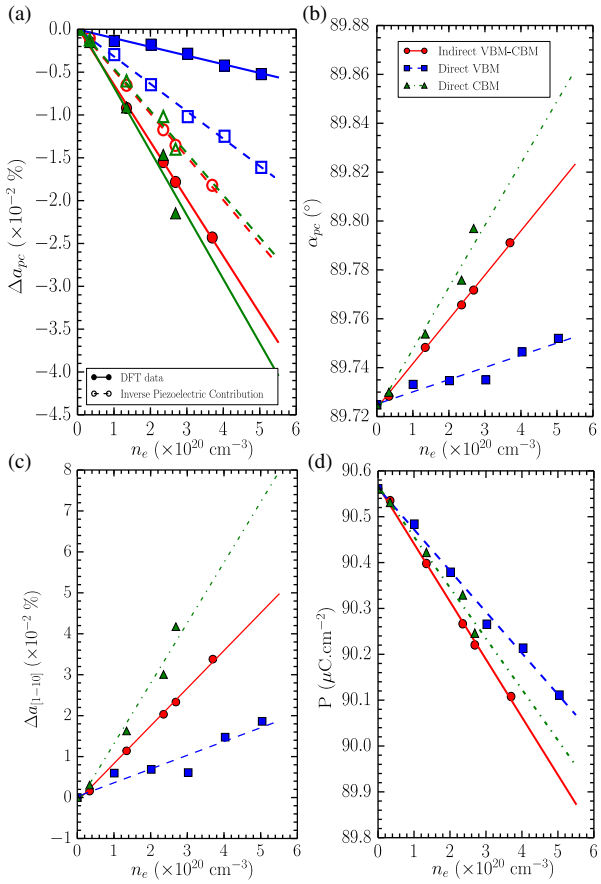

FIG. 2. Dependence of various properties on the n_e concentration of electrons excited in the conduction band states for the direct VBM (blue lines and data), the indirect VBM-CBM (red lines and data), and the direct CBM cases (green line and data), as predicted by the ΔSCF method. Panel (a) shows the relative change in pseudocubic lattice constant. Panel (b) reports the change in pseudocubic angle for the three transitions. Panel (c) shows the relative change in lattice constant along the $[1\bar{1}0]$ direction. Panel (d) shows the change of electrical polarization. Lines in all the panels are linear fits of the data (indicated by symbols). The open symbols and dashed lines in (a) display the estimated change of lattice constant arising from the inverse piezoelectric effect (see text).

pronounced for the direct CBM and indirect VBM-CBM cases than for the direct VBM transition, therefore, pointing out the importance of exciting electrons into the CBM to generate larger structural modifications with respect to the ground state.

Moreover, the behavior of a_{pc} and α_{pc} reported in Figs. 2(a) and 2(b), in fact, allows us to compute the dependence of the lattice constant along *any* direction as a function of n_e. For example, Fig. 2(c) indicates that the lattice expands along the pseudocubic $[1\bar{1}0]$ direction, which originates from the fast increase of the pseudocubic angle in Fig. 2(b) relative to the shrinking of the lattice constant shown in Fig. 2(a). In order to have more information about this directional dependency, Table I reports the relative

TABLE I. Relative change in lattice constant along different crystallographic directions for a concentration of excited electrons of 5×10^{18} electrons per cm^3.

$\Delta a/a$ ($\times 10^{-4}$%)	[100]	$[1\bar{1}0]$	[110]	$[1\bar{1}1]$	[111]
Indirect VBM-CBM	−3.3	+4.6	−11.2	+1.9	−24.2
Direct VBM	−0.5	+1.7	−2.7	+0.9	−6.1
Direct CBM	−3.7	+7.4	−14.7	+3.7	−32.7

change of lattice constant along different crystallographic directions, for concentration of excited electrons of 5×10^{18} electrons/cm^3 (such latter concentration is chosen in between the experimentally estimated value of 5×10^{17} cm^{-3} in BFO nanowires [31] and the largest estimate of 5×10^{19} cm^{-3} in Ref. [9]). Table I reveals that, for any of the three considered transitions, the lattice constant for directions being close to the polarization direction (such as pseudocubic [111] or [110]) shorten upon increasing the concentration of excited electrons. On the other hand, directions having a large angle with **P** (such as $[1\bar{1}0]$ or $[1\bar{1}1]$) exhibit a lattice constant that increases with n_e. Our calculations, therefore, indicate that it is crucial to precisely report the crystallographic direction when measuring the light-induced change in lattice constant. Regarding the magnitude of our predicted photostriction effect, our results for the direct VBM, indirect VBM-CBM, and direct CBM cases provide a relative change in lattice constant of $+1.7\times10^{-4}$%, $+4.6\times10^{-4}$%, and $+7.4\times10^{-4}$%, respectively, for the pseudocubic $[1\bar{1}0]$ direction (when choosing $n_e = 5 \times 10^{18}$ electrons per cm^3). These predictions are in rather good agreement with the expansion under illumination of $+15\times10^{-4}$% measured in Ref. [6] along a second-nearest neighbor direction—especially when recalling that n_e is not precisely known but rather estimated to be in between 5×10^{17} and 5×10^{19} cm^{-3}.

Let us now try to determine the microscopic mechanism responsible for the photostrictive effects. For that, Fig. 2(d) and Fig. 3(a) report the electrical polarization (as estimated from the product of Born effective charges of BFO ground state [24] and ionic displacements) [32] and the volume V of the primitive cell, as functions of n_e for all studied transitions. These two figures reveal that increasing the concentration of excited electrons quasilinearly reduces both polarization and volume, as qualitatively similar to the effect that hydrostatic pressure is known to have on the magnitude of **P** and on V [36,37]. One can therefore contemplate the idea that n_e plays the role of a pressure of electronic origin, induced by the transition of electrons from valence to conduction states [38]. However, the DFT data of Ref. [36] for BFO under hydrostatic pressure gives a linear variation of the relative volume as a function of the relative polarization of about 0.41 while Fig. 3(b) shows that this slope is about 0.03, 0.12, and 0.13 for the direct VBM, indirect VBM-CBM, and direct CBM cases. In other

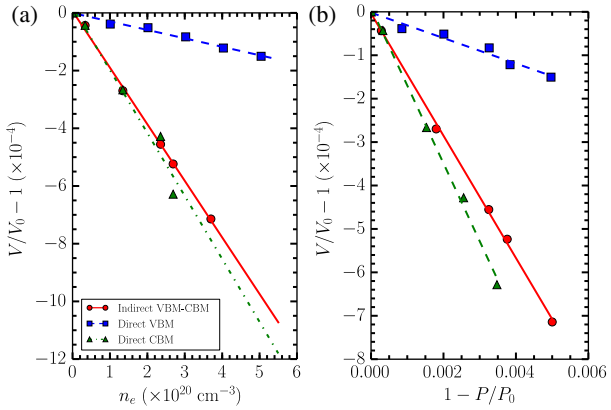

FIG. 3. Dependencies of the relative volume (with respect to the ground state) as a function of the excited electron concentration (a), and as a function of the relative change in polarization (b). Data are shown by means of symbols and lines are linear fits of such data. The blue squares, red circles, and green triangles represent the direct VBM, indirect VBM-CBM, and direct CBM cases, respectively.

words, this slope inherent to photostriction is about 13.7 times, 3.4 times and 3.2 times *smaller* for the direct VBM, indirect VBM-CBM, and direct CBM transitions, respectively, than the one associated with hydrostatic pressure. Such differences rule out the idea that photostriction is a sole electronic pressure induced effect.

Let us thus investigate another possibility to explain photostriction: the electrons excited in conduction band states screen the polarization, which is thus reduced. This is consistent with Fig. 2(d), indicating a decrease of polarization when increasing n_e. Note also that such screening should naturally depend on the conduction state of the excited electron, which is also consistent with Fig. 2(d) showing that the polarization of the direct CBM is similar to that of the indirect VBM-CBM, but differs from that of the direct VBM transition. This latter reduction of the polarization then generates a change in the lattice constant via the inverse piezoelectric effect,

$$\delta\eta_{ij} = g_{ijk}\delta P_k, \tag{2}$$

where $\delta\eta_{ij}$ are the components of the induced strain tensor, and δP_k is the change of the kth component of the polarization with respect to that of the ground state. g_{ijk} are elements of a third-rank tensor given by [42]

$$\boldsymbol{g} = \boldsymbol{d}^T.\boldsymbol{\chi}^{-1}, \tag{3}$$

where $\boldsymbol{d}^T$, the transposed piezoelectric tensor, relates the change of strain to an applied electric field [43,44] and $\boldsymbol{\chi}$ is the dielectric susceptibility.

In order to check such a scenario involving the inverse piezoelectric effect, we use the values of the elements of both $\boldsymbol{d}$ and $\boldsymbol{\epsilon}$ tensors computed in Ref. [45] at −200 °C, in order to practically obtain the elements of the $\boldsymbol{g}$ tensor of Eq. (3). These g_{ijk} coefficients are then multiplied by the change in polarization given by our own data displayed in Fig. 2(d). The resulting change of the pseudocubic lattice constant is reported as open symbols in Fig. 2(a) as a function of n_e, for the three transitions—in addition to that arising from the direct relaxation of the cell under the n_e constraint within the ΔSCF method (given in plain symbols). One can clearly see that our proposed scenario involving the inverse piezoelectric effect can account for the main part of the ΔSCF-computed lattice constant change variation in the case of the indirect VBM-CBM and direct CBM transitions, that is about 79% and 69%, respectively. The remaining amount may be due to a small contribution of the aforementioned electronic pressure, or contributions from polarons. It may also either arise from a slight underestimation of the piezoelectric and/or dielectric coefficients given in Ref. [45] for the ground state of BFO, or from the fact that these coefficients, as well as the Born effective charges we used to estimate the polarization, can also technically vary when free carriers are present [7]. These latter effects may also explain why the inverse piezoelectric scenario is estimated to yield a change in lattice constant that is 3 times larger than what is observed from the raw ΔSCF data for the direct VBM transition, as further indicated by Fig. 2(a)—especially, when realizing that the direct VBM transition, unlike the indirect VBM-CBM and direct CBM cases, involves a conduction state of much higher energy than the CBM state. Moreover, we found, by carrying additional calculations at fixed positions of the oxygen atoms, that preventing the oxygen octahedral tilting from responding to a change in exciting electron concentration reduces the photo-induced effects by 25% [46]—therefore highlighting the role of oxygen octahedra in BFO.

Early works interpreted the photostriction effect based on free carriers traveling to surfaces to screen the internal depolarizing fields [11,30], which is incompatible with subpicosecond photostriction experiments [10]. In contrast, the present work demonstrates that screening of the polarization at the level of the unit cell can generate a piezoelectric effect compatible with the observed change in lattice constant, even in the absence of migration of the photogenerated free carriers, thus resolving the aforementioned discrepancy. According to our results, photostriction effects shall, therefore, be observed in perfect short-circuit conditions, which is of great technological importance for integration in all-optical control electronic devices.

In summary, we introduced an *ab initio* procedure, based on the Δ SCF method, to tackle photostriction in ferroelectrics. This procedure, applied to the case of the multiferroic $BiFeO_3$, results in changes of lattice constant that have the same order of magnitude as those observed experimentally. The most significant contribution to photostriction in $BiFeO_3$ is a combination of polarization screening and inverse piezoelectric effect. This work further

opens a route towards designing highly photostrictive materials, by providing several guidelines. In order to enhance the photostriction phenomenon, one should look for polar materials for which the polarization can efficiently be screened by conduction electrons. We, therefore, encourage the use of many classical transition metal ABO_3 perovskites, such as $BaTiO_3$, for which the polarization and the conduction band are strongly dependent on the B site. Moreover, the analysis of our results strongly suggests that high piezoelectric-constant materials are recommended for large photostrictive effects. Solid solutions near their morphotropic phase boundary [47] are, therefore, promising in that regard, as consistent with the experimental finding of a relatively large photostriction in $(Pb, La)(Zr, Ti)O_3$ [48].

We thank Michel Viret for insightful discussions about the photostriction effect and Sahar Sharifzadeh for pointing out the use of constrained-DFT to study excited state geometry of solids. C. P. thanks a public grant overseen by the French National Research Agency (ANR) as part of the "Investissements d'Avenir" program (Reference: ANR-10-LABX-0035, Labex NanoSaclay). L. B. and B. X. thanks the support of the DARPA Grant No. HR0011-15-2-0038 (MATRIX program) and the Air Force Office of Scientific Research under Grant No. FA9550-16-1-0065. We also acknowledge the Arkansas High Performance Computer Center at the University of Arkansas for access to the supercomputers.

*charles.paillard@centralesupelec.fr

[1] C. Paillard, X. Bai, I. C. Infante, M. Guennou, G. Geneste, M. Alexe, J. Kreisel, and B. Dkhil, Adv. Mater., 10.1002/adma.201505215 (2016).
[2] S. Y. Yang, J. Seidel, S. J. Byrnes, P. Shafer, C.-H. Yang, M. D. Rossell, P. Yu, Y.-H. Chu, J. F. Scott, J. W. Ager, L. W. Martin, and R. Ramesh, Nat. Nanotechnol. **5**, 143 (2010).
[3] I. Grinberg, D. V. West, M. Torres, G. Gou, D. M. Stein, L. Wu, G. Chen, E. M. Gallo, A. R. Akbashev, P. K. Davies, J. E. Spanier, and A. M. Rappe, Nature (London) **503**, 509 (2013).
[4] T. M. Brenner, D. A. Egger, L. Kronik, G. Hodes, and D. Cahen, Nat. Rev. Mater. **1**, 15007 (2016).
[5] B. Kundys, Appl. Phys. Rev. **2**, 011301 (2015).
[6] B. Kundys, M. Viret, D. Colson, and D. O. Kundys, Nat. Mater. **9**, 803 (2010).
[7] B. Kundys, M. Viret, C. Meny, V. Da Costa, D. Colson, and B. Doudin, Phys. Rev. B **85**, 092301 (2012).
[8] P. Ruello, T. Pezeril, S. Avanesyan, G. Vaudel, V. Gusev, I. C. Infante, and B. Dkhil, Appl. Phys. Lett. **100**, 212906 (2012).
[9] M. Lejman, G. Vaudel, I. C. Infante, P. Gemeiner, V. E. Gusev, B. Dkhil, and P. Ruello, Nat. Commun. **5**, 4301 (2014).
[10] D. Schick, M. Herzog, H. Wen, P. Chen, C. Adamo, P. Gaal, D. G. Schlom, P. G. Evans, Y. Li, and M. Bargheer, Phys. Rev. Lett. **112**, 097602 (2014).
[11] D. Daranciang *et al.*, Phys. Rev. Lett. **108**, 087601 (2012).
[12] H. Wen, M. Sassi, Z. Luo, C. Adamo, D. G. Schlom, K. M. Rosso, and X. Zhang, Sci. Rep. **5**, 15098 (2015).
[13] P. Hohenberg and W. Kohn, Phys. Rev. **136**, B864 (1964).
[14] C. A. Ullrich, *Time-Dependent Density-Functional Theory, Concepts and Applications* (Oxford University Press, New York, 2012).
[15] L. Hedin, Phys. Rev. **139**, A796 (1965).
[16] A. Görling, Phys. Rev. A **59**, 3359 (1999).
[17] R. M. Martin, *Electronic Structure: Basic Theory and Practical Methods* (Cambridge University Press, Cambridge, England, 2004).
[18] J. Gavnholt, T. Olsen, M. Engelund, and J. Schiøtz, Phys. Rev. B **78**, 075441 (2008).
[19] K. Nakamura, Y. Kitaoka, T. Akiyama, T. Ito, M. Weinert, and A. J. Freeman, Phys. Rev. B **85**, 235129 (2012).
[20] Y. Kitaoka, K. Nakamura, T. Akiyama, T. Ito, M. Weinert, and A. J. Freeman, Phys. Rev. B **87**, 205113 (2013).
[21] X. Gonze *et al.*, Comput. Phys. Commun. **180**, 2582 (2009).
[22] M. Torrent, F. Jollet, F. Bottin, G. Zérah, and X. Gonze, Comput. Mater. Sci. **42**, 337 (2008).
[23] I. A. Kornev, S. Lisenkov, R. Haumont, B. Dkhil, and L. Bellaiche, Phys. Rev. Lett. **99**, 227602 (2007).
[24] J. B. Neaton, C. Ederer, U. V. Waghmare, N. A. Spaldin, and K. M. Rabe, Phys. Rev. B **71**, 9 (2004).
[25] F. Zavaliche, S. Y. Yang, T. Zhao, Y. H. Chu, M. P. Cruz, C. B. Eom, and R. Ramesh, Phase Transit. **79**, 991 (2006).
[26] P. Rovillain, M. Cazayous, Y. Gallais, A. Sacuto, R. P. S. M. Lobo, D. Lebeugle, and D. Colson, Phys. Rev. B **79**, 180411 (2009).
[27] W. Setyawan and S. Curtarolo, Comput. Mater. Sci. **49**, 299 (2010).
[28] Z. Zhang, Z. Jin, Q. Pan, Y. Xu, X. Lin, G. Ma, and Z. Cheng, Appl. Phys. Lett. **104**, 151902 (2014).
[29] M. Alexe, Nano Lett. **12**, 2193 (2012).
[30] H. Wen, P. Chen, M. P. Cosgriff, D. A. Walko, J. H. Lee, C. Adamo, R. D. Schaller, J. F. Ihlefeld, E. M. Dufresne, D. G. Schlom, P. G. Evans, J. W. Freeland, and Y. Li, Phys. Rev. Lett. **110**, 037601 (2013).
[31] K. Prashanthi, P. Dhandharia, N. Miriyala, R. Gaikwad, D. Barlage, and T. Thundat, Nano Energy **13**, 240 (2015).
[32] Note that experimental evidences on oxygen deficient $BaTiO_3$ [33,34] and theoretical investigation of charged $BaTiO_3$ cells [35] both demonstrate that a ferroelectric material is capable of retaining its polarization up to 1.9×10^{21} electrons per cm^3, as also consistent with the fact that *Wang et al.* showed that the relative anion-cation displacements are constant for moderate electron concentration, which is below 0.04 electron per unit cell [35].
[33] T. Kolodiazhnyi, M. Tachibana, H. Kawaji, J. Hwang, and E. Takayama-Muromachi, Phys. Rev. Lett. **104**, 147602 (2010).
[34] J. Hwang, T. Kolodiazhnyi, J. Yang, and M. Couillard, Phys. Rev. B **82**, 214109 (2010).
[35] Y. Wang, X. Liu, J. D. Burton, S. S. Jaswal, and E. Y. Tsymbal, Phys. Rev. Lett. **109**, 247601 (2012).

[36] S. Prosandeev, D. Wang, W. Ren, J.Íñiguez, and L. Bellaiche, Adv. Funct. Mater. **23**, 234 (2013).
[37] J. Buhot, C. Toulouse, Y. Gallais, A. Sacuto, R. de Sousa, D. Wang, L. Bellaiche, M. Bibes, A. Barthélémy, A. Forget, D. Colson, M. Cazayous, and M.-A. Measson, Phys. Rev. Lett. **115**, 267204 (2015).
[38] Note that we also numerically found (see Supplemental Material [39]) that the oxygen octahedral tilting slightly strengthens when increasing n_e, as also found for BFO under increasing hydrostatic pressure [36] and as consistent with the known repulsion between polarization and these tiltings [41]—i.e., a decrease in polarization magnitude [as the one shown in Fig. 2(d)] is typically accompanied with an enhancement in oxygen octahedral tiltings.
[39] See Supplemental Material at http://link.aps.org/supplemental/10.1103/PhysRevLett.116.247401 for further detail about the band structure under photoexcitation, charging the unit cell, influence of oxygen octahedra tilts, and the Landau model used, and includes Refs. [5,38,40].
[40] R. Pasynkov, Ferroelectrics **6**, 19 (1973).
[41] I. A. Kornev, L. Bellaiche, P.-E. Janolin, B. Dkhil, and E. Suard, Phys. Rev. Lett. **97**, 157601 (2006).
[42] D. Damjanovic, Rep. Prog. Phys. **61**, 1267 (1998).
[43] L. Bellaiche, Curr. Opin. Solid State Mater. Sci. **6**, 19 (2002).
[44] J. F. Nye, *Physical Properties of Crystals* (Oxford University Press, Oxford, 1985).
[45] M. Graf, M. Sepliarsky, R. Machado, and M. Stachiotti, Solid State Commun. **218**, 10 (2015).
[46] The Supplemental Material [39] provides further details about photostriction and related effects, such as the importance of tilting.
[47] S. Zhang, R. Xia, L. Lebrun, D. Anderson, and T. R. Shrout, Mater. Lett. **59**, 3471 (2005).
[48] P. Poosanaas and K. Uchino, Mater. Chem. Phys. **61**, 36 (1999).